Active control of scalar Helmholtz fields in the presence of known impenetrable obstacles

Lander Besabe and Daniel Onofrei

Abstract. In this paper, we consider the question of actively manipulating scalar Helmholtz fields radiated by a given source that is supported on a compact domain. We claim that the field radiated by the source approximates given scalar fields in prescribed exterior regions while maintaining desired far field patterns in prescribed directions in the presence of exterior known impenetrable obstacles. For simplicity of the exposition, we consider a simplified geometry with only one obstacle, one region of control, and a finite number of far field directions and present a theoretical argument for our claim stated above. Afterwards, we also show how it can be elementarily extended to the general case. Further, we construct a numerical scheme to compute these boundary inputs using the method of moments, the addition theorem, Tikhonov regularization, and Laplace spherical functions.

1. Introduction

1.1. General Background. The study of active control problems for fields modeled by the scalar Helmholtz equation is a very active area of research not only due to its intrinsic importance to acoustic wave phenomena but also because in many situations scalar problems can be used as an approximation to electromagnetic phenomena since they often preserve many important aspects of the problem while avoiding excessive mathematical complexities. In fact, for two-dimensional models, vector electromagnetic problems can be reduced to scalar formulations. Thus, there already exists a rich body of literature concerning the problem of active manipulation of vector and scalar fields in desired regions of space. The active (partial) nulling of acoustic fields was first studied in [**34**] (feed-forward control of sound) and in [**49**] (feedback control of sound). The works [**59**], [**25**], [**36**], [**39**], [**38**], [**37**], [**56**], [**23**], [**55**], [**63**], [**22**], [**3**] discuss methods and source optimization strategies for the active control of scalar fields modeled by the Helmholtz equation. Common applications include active noise cancellation ([**48**], [**24**], [**11**], [**32**], [**42**]), sound synthesis and reproduction ([**3**], [**30**], [**50**],[**68**],[**62**], [**17**]), and active control of acoustic scattered fields with application to cloaking and shielding ([**6**],

2010 *Mathematics Subject Classification.* Primary 35R30 , 35J05, 45Q05; Secondary 35R25, 45P05, 93C20, 31B10.

Key words and phrases. Active Cloaking, Helmholtz Equation, Integral equations.

[**67**], [**65**],[**66**],[**35**], [**20**], [**52**], [**41**]). A more comprehensive discussion and analysis of some of the methods employed in these applications is also given in [**10**] for scattered field control and in [**21**] and [**1**] for sound field synthesis.

There is an extensive literature on the active control of Helmholtz fields. In [**36**] and [**39**], active scalar Helmholtz controls were constructed through generalized Calderon potentials and boundary projection operators while in [**47**] and [**67**], the authors employed the Green representation theorem to characterize active controls for the scalar Helmholtz equation. Multizone field synthesis and reproduction were studied using wave-domain methods (such as in [**26**], [**27**]) or modal-domain approaches (see [**46**], [**69**]). An algorithm for the reduction of scattering interference to the overall multizone scalar field synthesis effect was presented in [**68**]. In [**51**] and [**52**] the author made use of boundary integral operators to produce a stable unified control strategy in the case of a single active surface source proving the active control of radiated scalar fields in prescribed exterior region of space. These theoretical results were later applied for the 2D and 3D numerical study in [**28**], [**53**], [**17**], [**18**]. Other ideas that are used in the context of Helmholtz field control are discussed and analyzed in [**4**], [**21**], [**58**] and [**70**]. The monographs [**29**], [**31**], [**9**] and [**7**] discuss at length the problem of scalar fields propagation in oceans and layered media.

The problem of far field synthesis requires the construction of necessary boundary inputs on the active sources for the approximation of a given far field pattern [**5**],[**2**] ("the far field synthesis") (see also the monograph of [**16**] where general radiation theory and source synthesis techniques are discussed). The works [**33, 14, 8, 15**] discuss the problem of pattern synthesis with prescribed exterior nulls in specified parts of the near field region. In [**61, 40**] the authors assume physical optics approximations (i.e., small wavelengths relative to the size of the obstacles) and consider obstacles positioned in specified subregions of the near field (see also the review [**12**], for a genetic optimization algorithm based on the far-field to near field mapping for a solution). In our formulation below, the active field control problem is formulated in homogeneous media in the presence of known impenetrable obstacles and it requires the characterization of optimal boundary inputs on the active sources for the approximation of various prescribed scalar fields in given exterior regions and specified far field directions.

Computational and analytical methods for scalar scattering and radiation are presented in many excellent monograph in the literature and we mention here just several major monographs, [**57, 64, 44**].

In this paper, we build up on our previous work and produce a theoretical result concerning the active control of radiated fields showing that we can approximate given scalar fields in prescribed exterior regions and given far field directions in the presence of known impenetrable obstacles. The paper is organized as follows: In the first part of Section 2 we introduce our main question and present the mathematical formulation of the main problem we solve. Then , in the second part of the section we present the argument leading to our main result. In Section 3 we show several numerical results to support our theoretical findings. The last Section presents our conclusions and remarks about future works.

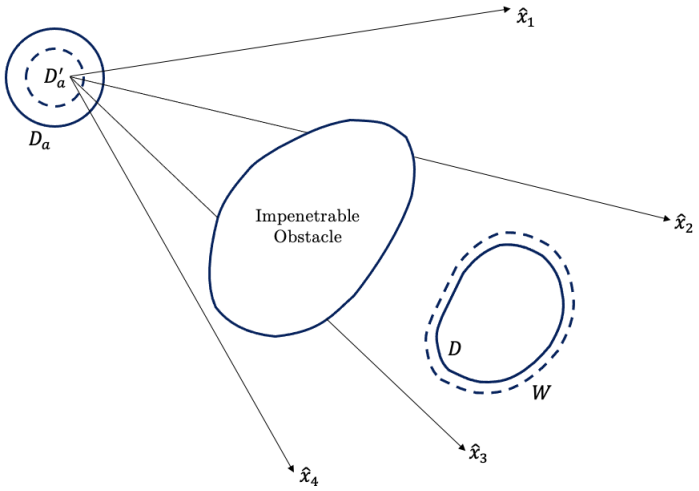

FIGURE 1. Sketch of the problem geometry

2. Statement of the Problem

The main question we plan to address concerns the characterization of physical boundary inputs on a given source support so that the radiated scalar field approximates desired behaviors in prescribed mutually disjoint exterior regions of space and desired far-field patterns in prescribed far-field directions in the presence of known exterior impenetrable obstacles.

For the simplicity of exposition while preserving the generality of the argument (see Remarks 2.2, 2.3, 2.4, 2.5), we will next consider the case where only one sound-soft obstacle is present with only one exterior control region and N far-field directions. See Figure 1 for a sketch of the geometry where only four far-field directions are drawn.

For the mathematical formulation of the problem, we need to introduce several notations. Let D_a be a compact smooth domain representing the physical source support. Consider D a compact control region and O be the open smooth set representing the sound-soft obstacle. Also, let $\hat{\mathbf{x}}_1, \hat{\mathbf{x}}_2, \ldots, \hat{\mathbf{x}}_N$ be unit vectors designating the N given far-field directions. As in one of the previous works, see [**52, 51, 53, 17, 54, 18**], we assume a fictitious source domain $D'_a \subset\subset D_a$ and a fictitious control domain $W \supset\supset D$ so that

$$\overline{D_a} \cap \overline{W} = \emptyset, \left(\overline{D_a} \cup \overline{W}\right) \cap \overline{O} = \emptyset,$$

where $\subset\subset$ denotes compact embedding. Without restricting the generality, we also assume that the non-physical fictitious domains D'_a and W are smooth. Mathematically, the problem can be formulated as follows. Consider the incident field $u_{inc}(\mathbf{x}) = \int_{\partial D'_a} w(\mathbf{y})\Phi(\mathbf{x},\mathbf{y})\, dS_y$ and assume there is no coupling between the obstacle O and the source D_a, e.g., the obstacle is in the far-field of the source. Let $0 < \mu \ll 1$, u_1 be a Helmholtz potential in W, $f_1, f_2, \ldots, f_N$ be given complex numbers. The problem is to determine the density w such that the total field u

obtained (radiated and scattered), i.e., $u = u_{inc} + u_s$ where u_s solves

$$\begin{cases} \Delta u_s + k^2 u_s = 0, & \text{in } \mathbb{R}^3 \setminus \overline{O} \\ \langle \frac{\mathbf{x}}{|\mathbf{x}|}, \boldsymbol{\nabla} u_s(\mathbf{x}) \rangle - iku_s(\mathbf{x}) = o\left(\frac{1}{|x|}\right), & \text{uniformly for all } \frac{\mathbf{x}}{|\mathbf{x}|} \text{ as } \mathbf{x} \to \infty \\ u_s = -u_{inc}, & \text{on } \partial O. \end{cases} \tag{2.1}$$

satisfies

$$\begin{cases} \|u - u_1\|_{L^2(\partial W)} < \mu \\ |u_\infty(\hat{\mathbf{x}}_i) - f_i| < \mu, \qquad \text{for } i = 1, \dots, N \end{cases} \tag{2.2}$$

where $u_\infty(\hat{\mathbf{x}}_i)$ denotes the far-field pattern of u in the direction of the unit vector $\hat{\mathbf{x}}_i$, $i = 1, \dots, N$.

Classical results [**13, 43, 45**] imply the existence of a unique solution. For simplicity, assuming k is not a Helmholtz Dirichlet eigenvalues for the interior problem in W, O, and D_a'. We look for u_s in the form of a double-layer potential

$$u_s(\mathbf{z}) = \int_{\partial O} v(\mathbf{y}) \frac{\partial \Phi}{\partial \nu_{\mathbf{y}}}(\mathbf{z}, \mathbf{y}) \, dS_{\mathbf{y}}, \quad \text{for } z \in \mathbb{R}^3 \setminus \partial O, \tag{2.3}$$

where $\Phi(\mathbf{x}, \mathbf{y}) = \frac{e^{ik|\mathbf{x}-\mathbf{y}|}}{4\pi|\mathbf{x}-\mathbf{y}|}$ is the fundamental solution of the 3D Helmholtz equation. Imposing the boundary condition on ∂O and using the jump of the double-layer potential operator, we get that v satisfies

$$\left(\mathcal{K}_O + \frac{1}{2} I\right) v = -\mathcal{P}_O w, \quad \text{on } \partial O,$$

where $\mathcal{K}_O : L^2(\partial O) \to L^2(\partial O)$ and $\mathcal{P}_O : L^2(\partial D_a') \to L^2(\partial O)$ are given by

$$\mathcal{K}_O v(\mathbf{x}) = \int_{\partial O} v(\mathbf{x}) \frac{\partial \Phi}{\partial \nu_y}(\mathbf{x}, \mathbf{y}) \, dS_{\mathbf{y}}, \quad \mathbf{x} \in \partial O,$$

and

$$\mathcal{P}_O w(\mathbf{z}) = \int_{\partial D_a'} w(\mathbf{y}) \Phi(\mathbf{x}, \mathbf{y}) \, dS_{\mathbf{y}}, \quad \mathbf{z} \in \partial O,$$

respectively. Then, since k is not a resonance, we get

$$v = -\left(\mathcal{K}_O + \frac{1}{2} I\right)^{-1} \mathcal{P}_O w$$

and

$$u_s(\mathbf{z}) = -\int_{\partial O} \left(\mathcal{K}_O + \frac{1}{2} I\right)^{-1} \mathcal{P}_O w(\mathbf{y}) \frac{\partial \Phi}{\partial \nu_{\mathbf{y}}}(\mathbf{z}, \mathbf{y}) \, dS_{\mathbf{y}}.$$

Then the total field in W is given by

$$\begin{aligned} u(\mathbf{z}) &= u_{inc}(\mathbf{z}) + u_s(\mathbf{z}) \\ &= \mathcal{P}_W w(\mathbf{z}) - \mathcal{D}_{O,W} \left(\mathcal{K}_O + \frac{1}{2} I\right)^{-1} \mathcal{P}_O w(\mathbf{z}), \end{aligned}$$

where $\mathcal{P}_W : L^2(\partial D_a') \to L^2(\partial W)$ and $\mathcal{D}_{O,W} : L^2(\partial O) \to L^2(\partial W)$ are defined by

$$\begin{aligned} \mathcal{P}_W w(\mathbf{z}) &= \int_{\partial D_a'} w(\mathbf{y}) \Phi(\mathbf{z}, \mathbf{y}) \, dS_{\mathbf{y}}, \quad z \in \partial W, \\ \mathcal{D}_{O,W} g(\mathbf{z}) &= \int_{\partial O} g(\mathbf{y}) \frac{\partial \Phi}{\partial \nu_{\mathbf{y}}}(\mathbf{z}, \mathbf{y}) \, dS_{\mathbf{y}}, \quad z \in \partial W, \quad \text{for } g \in L^2(\partial O). \end{aligned} \tag{2.4}$$

Moreover, the total field in the far-field direction $\hat{\mathbf{x}}_i$ is given by

(2.5)
$$u_\infty(\hat{\mathbf{x}}_i) = \frac{1}{4\pi}\int_{\partial D_a'} w(\mathbf{y}) e^{-ik\hat{\mathbf{x}}_i\cdot\mathbf{y}}\, dS_{\mathbf{y}} - \frac{1}{4\pi}\int_{\partial O}\left(\mathcal{K}_O + \frac{1}{2}I\right)^{-1}\mathcal{P}_O w(\mathbf{y})\frac{\partial e^{-ik\hat{\mathbf{x}}_i\cdot\mathbf{y}}}{\partial \nu_{\mathbf{y}}}\, dS_{\mathbf{y}}$$

for $i = 1, \dots N$. Hence, we can now introduce the total propagator operator $\mathcal{T} : L^2(\partial D_a') \to L^2(\partial W) \times \mathbb{C}^N$ by

$$\mathcal{T}w = \left(\mathcal{P}_W w(\mathbf{z}) - \mathcal{D}_{O,W}\left(\mathcal{K}_O + \frac{1}{2}I\right)^{-1}\mathcal{P}_O w(\mathbf{z}), u_\infty(\hat{\mathbf{x}}_1), \dots, u_\infty(\hat{\mathbf{x}}_N)\right) \tag{2.6}$$

where $\mathcal{P}_W$ and $\mathcal{D}_{O,W}$ are defined in (2.4) and u_∞ is defined in (2.5).

THEOREM 2.1. *The operator $\mathcal{T}$ defined above has a dense range.*

PROOF. To show this, since $\mathcal{T}$ is linear and compact, it suffices to show that $\ker \mathcal{T}^* = \{0\}$ where $\ker \mathcal{T}^*$ denotes the kernel of the adjoint operator T^*. The adjoint operator $\mathcal{T}^* : L^2(\partial W) \times \mathbb{C}^N \to L^2(\partial D_a')$ is given by

$$\langle \mathcal{T}w, \tilde{\psi}\rangle_{L^2(\partial W)\times\mathbb{C}^N} = \langle w, \mathcal{T}^*\tilde{\psi}\rangle_{L^2(\partial D_a')}$$

where $\tilde{\psi} = (\psi, c_1, \dots, c_N)$,

$$\langle \psi_1, \psi_2\rangle_{L^2(\partial W)} = \int_{\partial W}\psi_1\overline{\psi_2}$$

and

$$\langle (c_1, c_2, \dots, c_N), (d_1, d_2, \dots, d_N)\rangle_{\mathbb{C}^N} = \sum_{i=1}^N c_i\bar{d}_i$$

for every $\psi_1, \psi_2 \in L^2(\partial W)$ and $(c_1, c_2, \dots, c_N), (d_1, d_2, \dots, d_N) \in \mathbb{C}^N$. With these, we get

$$\begin{aligned}
\langle Tw, \tilde{\psi}\rangle_{L^2(\partial)\times\mathbb{C}^N} &= \left\langle \mathcal{P}_W w(\mathbf{z}) - \mathcal{D}_{O,W}\left(\mathcal{K}_O + \frac{1}{2}I\right)^{-1}\mathcal{P}_O w, \psi\right\rangle_{L^2(\partial W)} \\
&\quad + \sum_{i=1}^N u_\infty(\hat{x}_i)\cdot\bar{c}_i \\
&= \left\langle w, \mathcal{P}_W^*\psi - \mathcal{P}_O^*\left(\mathcal{K}_O' + \frac{1}{2}I\right)^{-1}\mathcal{D}_{O,W}^*\psi\right\rangle_{L^2(\partial D_a')} \\
&\quad + \sum_{i=1}^N \frac{1}{4\pi}\left[\int_{\partial D_a'} w(\mathbf{y}) e^{-ik\hat{\mathbf{x}}_i\cdot\mathbf{y}}\, dS_{\mathbf{y}}\right. \\
&\quad \left. - \int_{\partial O}\left(\mathcal{K}_O + \frac{1}{2}I\right)^{-1}\mathcal{P}_O w(\mathbf{z})\frac{\partial e^{-ik\hat{\mathbf{x}}_i\cdot\mathbf{z}}}{\partial \nu_{\mathbf{z}}}\, dS_{\mathbf{z}}\right]\cdot\bar{c}_i
\end{aligned} \tag{2.7}$$

where $\mathcal{P}_W^* : L^2(\partial W) \to L^2(\partial D_a')$ is the adjoint of $\mathcal{P}_W$ given by

$$\mathcal{P}_W^*\psi(\mathbf{y}) = \int_{\partial W}\psi(\mathbf{z})\overline{\Phi}(\mathbf{z}, \mathbf{y})\, dS_{\mathbf{z}}, \quad \mathbf{y} \in \partial D_a',$$

$\mathcal{P}_O^* : L^2(\partial O) \to L^2(\partial D_a')$ is the adjoint of $\mathcal{P}_O$ defined by

$$\mathcal{P}_O^*\xi(\mathbf{y}) = \int_{\partial O}\xi(\mathbf{z})\overline{\Phi}(\mathbf{z}, \mathbf{y})\, dS_{\mathbf{z}}, \quad \mathbf{y} \in \partial D_a',$$

$\mathcal{K}'_O : L^2(\partial O) \to L^2(\partial O)$ is the adjoint of $\mathcal{K}_O$ given in [**13**],

$$\mathcal{K}'_O \xi(\mathbf{x}) = \int_{\partial O} \xi(\mathbf{y}) \overline{\frac{\partial \Phi}{\partial \nu_{\mathbf{y}}}}(\mathbf{x}, \mathbf{y}) \, dS_{\mathbf{y}}, \quad \mathbf{y} \in \partial O,$$

and lastly, $\mathcal{D}^*_{O,W} : L^2(\partial W) \to L^2(\partial O)$ is the adjoint of $\mathcal{D}_{O,W}$ given by

$$\mathcal{D}^*_{O,W} \psi(\mathbf{y}) = \int_{\partial W} \psi(\mathbf{z}) \overline{\frac{\partial \Phi}{\partial \nu_{\mathbf{y}}}}(\mathbf{z}, \mathbf{y}) \, dS_{\mathbf{y}}, \quad \mathbf{z} \in \partial O.$$

So, algebraic manipulation of (2.7) gives

(2.8)

$$\begin{aligned} \langle Tw, \tilde{\psi} \rangle_{L^2(\partial) \times \mathbb{C}^N} = & \left\langle w, \left(\mathcal{P}^*_W - \mathcal{P}^*_O \left(\mathcal{K}'_O + \frac{1}{2} I \right)^{-1} \mathcal{D}^*_{O,W} \right) \psi \right\rangle_{L^2(\partial D'_a)} \\ & + \int_{\partial D'_a} w(\mathbf{y}) \overline{\sum_{i=1}^N \frac{1}{4\pi} \left(e^{ik\hat{\mathbf{x}}_i \cdot \mathbf{y}} - \mathcal{P}^*_O \left(\mathcal{K}'_O + \frac{1}{2} I \right)^{-1} \frac{\partial e^{ik\hat{\mathbf{x}}_i \cdot \mathbf{z}}}{\partial \nu_{\mathbf{z}}} \, dS_{\mathbf{z}} \right) \cdot c_i}, \end{aligned}$$

where $\frac{\partial e^{ik\hat{\mathbf{x}}_i \cdot \mathbf{z}}}{\partial \nu_{\mathbf{z}}}$ is considered defined for $\mathbf{z} \in \partial O$. Consequently, from (2.8), we obtain

$$\begin{aligned} \mathcal{T}^* \tilde{\psi}(\mathbf{y}) = & \left(\left(\mathcal{P}^*_W - \mathcal{P}^*_O \left(\mathcal{K}'_O + \frac{1}{2} I \right)^{-1} \mathcal{D}^*_{O,W} \right) \psi \right) (\mathbf{y}) \\ & + \frac{1}{4\pi} \sum_{i=1}^N \left(e^{ik\hat{\mathbf{x}}_i \cdot \mathbf{y}} - \mathcal{P}^*_O \left(\mathcal{K}'_O + \frac{1}{2} I \right)^{-1} \left(\frac{\partial e^{ik\hat{\mathbf{x}}_i \cdot \mathbf{z}}}{\partial \nu_{\mathbf{z}}} \right) (\mathbf{y}) \right) \cdot c_i, \end{aligned} \tag{2.9}$$

for $\mathbf{y} \in \partial D'_a$ Now, we define

$$\begin{aligned} f(\mathbf{x}) = & \int_{\partial W} \psi(\mathbf{y}) \bar{\Phi}(\mathbf{x}, \mathbf{y}) \, dS_{\mathbf{y}} - \int_{\partial O} \left(\mathcal{K}'_O + \frac{1}{2} I \right)^{-1} \mathcal{D}^*_{O,W} \psi(\mathbf{z}) \bar{\Phi}(\mathbf{x}, \mathbf{z}) \, dS_{\mathbf{z}} \\ & + \frac{1}{4\pi} \sum_{i=1}^N \left(e^{ik\hat{\mathbf{x}}_i \cdot \mathbf{x}} - \int_{\partial O} \left(\mathcal{K}'_O + \frac{1}{2} I \right)^{-1} \frac{\partial e^{ik\hat{\mathbf{x}}_i \cdot \mathbf{z}}}{\partial \nu_{\mathbf{z}}} \bar{\Phi}(\mathbf{x}, \mathbf{z}) \, dS_{\mathbf{z}} \right) \cdot c_i, \end{aligned} \tag{2.10}$$

for $\mathbf{x} \in \overline{D'_a}$. For $\tilde{\psi} = (\psi, c_1, \ldots, c_N) \in \ker \mathcal{T}^*$, from (2.9) and (2.10),

$$f(\mathbf{y}) = \mathcal{T}^* \tilde{\psi}(\mathbf{y}), \quad \mathbf{y} \in \partial D'_a$$

and thus, f solves the homogeneous Dirichlet problem in D'_a. Therefore, since k is not an interior Helmholtz Dirichlet eigenvalue for D'_a, using uniqueness, we have that

$$f = 0 \text{ on } D'_a,$$

and analytic continuation implies

$$f = 0 \text{ in } \mathbb{R}^3 \setminus \left(\overline{W} \cup \overline{O} \right). \tag{2.11}$$

Continuity of the single-layer implies $f = 0$ on $\partial W \cup \partial O$. Since f satisfies the Helmholtz homogeneous equation in W and k is not an interior Helmholtz Dirichlet eigenvalue in W, from (2.11) and uniqueness of the interior Dirichlet problem in W, we get

$$f = 0 \text{ in } \overline{W}. \tag{2.12}$$

Using the jump relation of the normal derivatives of the single-layer operator on ∂W, we obtain

$$\psi = 0 \text{ on } \partial W. \tag{2.13}$$

Using (2.13) in (2.10), we get

$$f(\mathbf{x}) = \frac{1}{4\pi}\sum_{i=1}^{N}\left(e^{ik\hat{\mathbf{x}}_i\cdot\mathbf{x}} - \int_{\partial O}\left(\mathcal{K}_O' + \frac{1}{2}I\right)^{-1}\frac{\partial e^{ik\hat{\mathbf{x}}_i\cdot\mathbf{z}}}{\partial \nu_{\mathbf{z}}}\bar{\Phi}(\mathbf{x},\mathbf{z})\,dS_{\mathbf{z}}\right)\cdot c_i. \tag{2.14}$$

From (2.11) and (2.12), we derive

$$f = 0 \text{ in } \mathbb{R}^3 \setminus \overline{O}. \tag{2.15}$$

Continuity of the single-layer potential on ∂O gives

$$f = 0 \text{ on } \partial O. \tag{2.16}$$

Since f satisfies the homogeneous Helmholtz equation in O and k is not an interior Helmholtz Dirichlet eigenvalue in O, relation (2.16) and uniqueness of the interior Dirichlet problem in O implies

$$f = 0 \text{ in } O. \tag{2.17}$$

Using again the jump relations of the normal derivatives of the single-layer potential on ∂O, we obtain from (2.15) and (2.17),

$$\sum_{i=1}^{N}\left(\mathcal{K}_O' + \frac{1}{2}I\right)^{-1}\frac{\partial e^{ik\hat{\mathbf{x}}_i\cdot\mathbf{z}}}{\partial \nu_{\mathbf{z}}}\cdot c_i = 0 \text{ on } \partial O. \tag{2.18}$$

With (2.18) in (2.14), (2.15), (2.16), (2.17), we have

$$f(\mathbf{y}) = \frac{1}{4\pi}\sum_{i=1}^{N} e^{ik\hat{\mathbf{x}}_i\cdot\mathbf{y}}c_i = 0 \text{ in } \mathbb{R}^3, \quad \text{for all } \mathbf{y}\in\mathbb{R}^3. \tag{2.19}$$

Proceeding as in [**19**], we first fix a unit vector $\mathbf{y}\in\mathbb{R}^3$ and define $\mathbf{y}_p = p\mathbf{y}$ for $p = 0,\ldots,N-1$ so that from (2.19), we obtain the Vandermonde system

$$\underbrace{\begin{bmatrix} 1 & 1 & \cdots & 1 \\ z_1 & z_2 & \cdots & z_N \\ \vdots & \vdots & \ddots & \vdots \\ z_1^{N-1} & z_2^{N-1} & \cdots & z_N^{N-1} \end{bmatrix}}_{:=Z}\begin{bmatrix} c_1 \\ c_2 \\ \vdots \\ c_N \end{bmatrix} = \begin{bmatrix} 0 \\ 0 \\ \vdots \\ 0 \end{bmatrix} \tag{2.20}$$

where $z_i = e^{ik\hat{\mathbf{x}}_i\cdot\mathbf{y}}$. The unique solution of (2.20) is the trivial solution where $c_i = 0$ for all $i = 1,\ldots,N$ whenever the coefficient matrix Z is nonsingular. The determinant of the Vandermonde matrix above is given by

$$det(Z) = \prod_{1\le j\le 1\le N}(z_j - z_i) \tag{2.21}$$

which is zero if and only if at least one of the differences in the product is zero, i.e., there are indices j_1, j_2 such that $z_{j_1} = z_{j_2}$, equivalently this means that

$$(\hat{\mathbf{x}}_{j_1} - \hat{\mathbf{x}}_{j_2})\cdot\mathbf{y} = \frac{2\pi}{k}M \tag{2.22}$$

for some integer M. Hence, we get $|M| = \frac{k}{2\pi}|(\hat{\mathbf{x}}_{j_1} - \hat{\mathbf{x}}_{j_2})\cdot\mathbf{y}| \le \frac{k}{\pi}$ by triangle inequality and Cauchy-Schwarz inequality. This means that choosing $\mathbf{y}$ on the

exterior of the hyperplanes defined by $\begin{pmatrix} N \\ 2 \end{pmatrix} \left(2\lfloor \frac{k}{\pi} \rfloor + 1\right)$ equations of the form (2.22), we observe that this gives a set of N $\mathbf{y}$ values, which are the $\mathbf{y}_p$ vectors, that results to (2.19) having the solution $c_i = 0$ for all $i = 1, \ldots, N$ and thus, $\mathcal{T}$ has a dense range. □

REMARK 2.2. Note that the physical source input on ∂D_a is obtained from u_{inc} introduced above either as pressure

$$p(\mathbf{x}) = \int_{\partial D_a'} w(\mathbf{y}) \Phi(\mathbf{x}, \mathbf{y}) \, dS_{\mathbf{y}} \tag{2.23}$$

for $\mathbf{x} \in \partial D_a$ or normal velocity

$$v(\mathbf{x}) = \frac{-i}{\rho c k} \frac{\partial}{\partial \nu_{\mathbf{x}}} \int_{\partial D_a'} w(\mathbf{y}) \Phi(\mathbf{x}, \mathbf{y}) \, dS_{\mathbf{y}} \tag{2.24}$$

for $\mathbf{x} \in \partial D_a$ where ρ denotes the density of the surrounding medium and c denotes the speed of propagation of sound in the respective media.

REMARK 2.3. It can be immediately seen that by using a single layer representation of the scattered field, the arguments presented in Theorem 2.1 can be adapted to the case when a sound-hard obstacle is used.

REMARK 2.4. We use a smooth fictitious source $D_a' \subset\subset D_a$ which simplifies the computation (we assume D_a' is a spherical domain) and ensures that, the boundary inputs given in Remark 2.2 will be smooth.

REMARK 2.5. By employing interior stability estimates, it was shown in [**52**] that L^2-control in ∂W is enough to show smooth interior control. Thus, we have that $\|u - u_1\|_{L^2(D)} < \epsilon$ for some $0 < \epsilon \ll 1$.

REMARK 2.6. If coupling between the obstacle is neglected then the theoretical argument presented in Theorem 2.1 extend immediately to the case of more impenetrable obstacles of the same type and also to the case where one has sound-soft and sound-hard obstacles (in this case, the well-posedness is implied by [**60**]).

REMARK 2.7. The arguments of Theorem 2.1 can be extended to all possible values of k which are made by considering a modified Green's function on a modified layer potential approach in the spirit of [**45**] and [**60**].

3. Numerical Implementation

In this section, we demonstrate a numerical scheme to support the theoretical concepts presented in the previous section. We consider problem (2.1), without far-field constraints, which may be summarized by finding a function $w \in L^2(D_a')$ such that

$$\mathcal{T} w = f \tag{3.1}$$

for a prescribed field $f = (f_1, \ldots, f_m) \in Y$, where $\mathcal{T}$ is defined in (2.6), with no far-field direction. In this numerical scheme, we will be using N point sources $\mathbf{y}_j$, $j = 1, \ldots, N$, which may be viewed as a discretization of the compact source D_a' described in the previous section or in their own as suggested by the following numerical results, a spherical sound-soft obstacle O, and a control region W. Note that we set the center of the obstacle as the center of the reference 3D system in

this implementation. We solve (3.1) by discretizing the control region into a mesh of M collocation points $\mathbf{z}_p$, $p = 1, \ldots, M$ and using far-field approximation and spherical harmonics to represent the density w. Hence, we transform (3.1) into a linear system

$$A_d w_d \approx b \tag{3.2}$$

where A_d is the $M \times N$ coefficient matrix of moments, M is the number of control points and N is the number of point sources we consider. We compute w_d as the Tikhonov solution

$$w_d = (\alpha I + A_d^* A_d)^{-1} A_d^* b, \tag{3.3}$$

where $0 < \alpha \ll 1$ is computed using Morozov discrepancy principle, which is a method to find an optimal parameter $\alpha > 0$ such that

$$\|A_d w_d - b\|_{\ell^2} = \delta,$$

for some accuracy criterion $0 < \delta \ll 1$ and A_d^* is the conjugate transpose of A_d.

3.1. Point sources are placed at least 10 wavelengths from the obstacle and are close to the control region. In this simulation, we assume that the obstacle is a sphere of radius R centered at the origin which is in the far field of the point sources. Thus, as developed in [**13**], where using the far-field approximation, i.e., $|\mathbf{y}_j| \gg 1$

$$u_{inc}(\mathbf{x}) = \sum_{j=1}^{N} w_j \frac{e^{ik|\mathbf{x}-\mathbf{y}_j|}}{4\pi|\mathbf{x}-\mathbf{y}_j|} \approx \sum_{j=1}^{N} w_j \underbrace{\frac{e^{ik|\mathbf{y}_j|}}{|\mathbf{y}_j|}}_{:=d_j} e^{-ik\hat{\mathbf{y}_j}\cdot\hat{\mathbf{x}}\cdot R}, \quad \text{for } \mathbf{x} = R\cdot\hat{\mathbf{x}} \in \partial O \tag{3.4}$$

where w_j are scalar entries of the (acoustic) density vector representing each point source $\mathbf{y}_j$ and R is the radius of the sound-soft obstacle O. By using (3.4) and the addition theorem for the spherical harmonic representation of plane waves, see [**13**], we obtain

$$u_{inc}(\mathbf{x}) = \sum_{j=1}^{N} w_j \frac{e^{ik|\mathbf{x}-\mathbf{y}_j|}}{4\pi|\mathbf{x}-\mathbf{y}_j|} \approx \sum_{j=1}^{N} 4\pi w_j d_j \sum_{n=0}^{\infty}\sum_{m=-n}^{n} i^n j_n(kR) Y_n^m(\hat{\mathbf{x}})\overline{Y_n^m(-\hat{\mathbf{y}_j})} \tag{3.5}$$

where j_n is the regular spherical Bessel function of order n and Y_n^m are the spherical harmonics. On the other hand, it is know that

$$u_s(\mathbf{z}) = \sum_{n=0}^{\infty}\sum_{m=-n}^{n} a_{mn} h_n^{(1)}(k|\mathbf{z}|) Y_n^m(\hat{\mathbf{z}}), \quad \mathbf{z} \in \mathbb{R}^3 \setminus O \tag{3.6}$$

where $h_n^{(1)}$ is the spherical Hankel function of order n. Using (3.4) – (3.6), the fact that $u_{inc}(\mathbf{x}) = -u_s(\mathbf{x})$ on ∂O, and orthogonality of the spherical harmonics, we get that the coefficients a_{mn} are computed by

$$a_{mn} = -4\pi i^n \frac{j_n(kR)\sum_{j=1}^{N} d_j \overline{Y_n^m(-\hat{\mathbf{y}_j})} w_j}{h_n^{(1)}(kR)}. \tag{3.7}$$

Now, we know that the total field u is given by $u(\mathbf{z}) = u_{inc}(\mathbf{z}) + u_s(\mathbf{z})$, where u_{inc} is the exact expression of the incident field, i,.e, the first equality, given in (3.5) and u_s is given by (3.6), (3.7).

In all the following simulations, we use the wave number $k = 10$ with direction of propagation $\hat{\mathbf{k}} = [1, 0, 0]$, and a spherical obstacle with radius $R = 1$. We also approximate the acoustic field using 30 harmonic orders, for a total of 961 spherical harmonics, and $N = 150$ point sources, and in this section, we set the point sources as points around a sphere of radius 0.7 centered at [4,-4,-4] so that we set the point sources at least 10 wavelengths away from the obstacle and we define the control region as

$$W = \left\{ (r, \theta, \phi) \in \mathbb{R}^3 : r \in [1, 1.5], \theta \in \left[-\frac{\pi}{8}, \frac{\pi}{10} \right], \phi \in \left[\frac{49\pi}{128}, \frac{79\pi}{128} \right] \right\}. \tag{3.8}$$

shifted to $[4.25, -4, -4]$ so that the region is one wavelength away from the sources, and represent it with 580 control points. Figure 2 shows the geometry of the problem (where a 2D sketch of the 3D geometry is rendered).

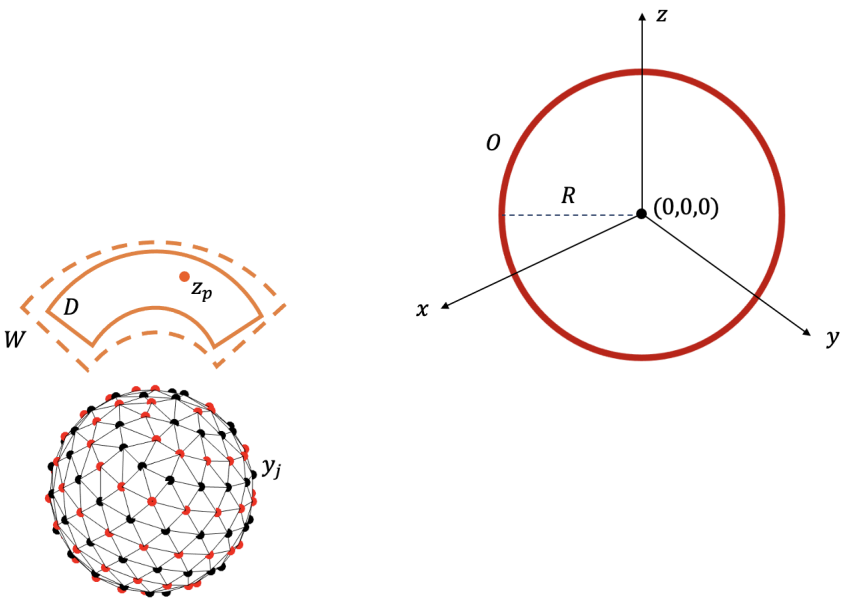

FIGURE 2. Geometry of the numerical scheme

We prescribe a field on W using a plane wave $f(\mathbf{z}) = e^{k \cdot \hat{\mathbf{k}} \cdot \mathbf{z}}$, for $\mathbf{z} \in W$. Since we represent W a set of 580 control points, we let $\mathbf{z} = \mathbf{z}_p$ for $p = 1, \ldots, 580$. Figure 3 shows the real parts of the generated field and the prescribed field on a mesh of W (which is different than the computational mesh of W), and the pointwise relative error on each point $\mathbf{z}_p$. We further note that in this particular simulation, maximum relative error on W is 0.39%. We further reiterate that the figures concerning W are on a slightly shifted mesh of W.

We then indicate the ℓ^2 norm of w_d, which is an indication of the power radiated by the point sources. In this simulation is $\|w_d\|_{\ell^2} = 8.6021$. Figure 4 shows the contribution, in magnitude, of each point source $\mathbf{y}_j$ for the source strength. In Figure 5, we exhibit the interpolated prescribed and generated fields on the $x = 5.40$ cross section of the control region W.

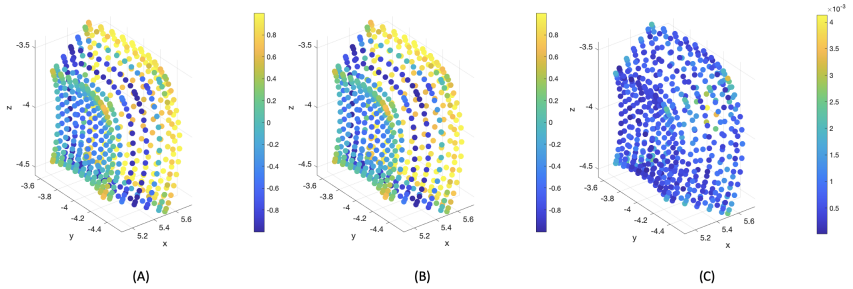

FIGURE 3. Real parts of the (A) generated and (B) desired fields on a shifted mesh of W, and (C) the pointwise relative error on W

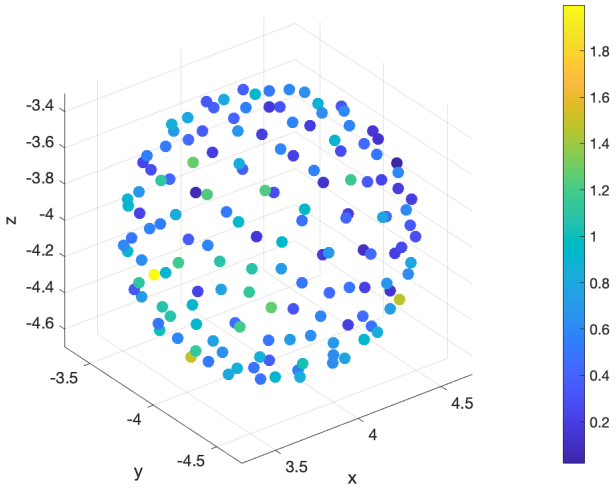

FIGURE 4. Power radiated by each point source $\mathbf{y}_j$ (magnitude)

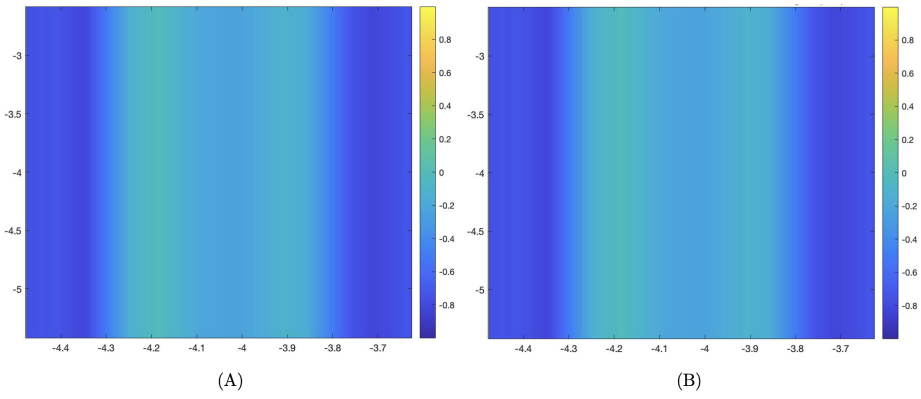

FIGURE 5. (A) Desired and (B) generated fields on a cross section of W

Next, moving the control region to two wavelengths away from the source by setting its center to $[5, -4, -4]$, the numerical simulation shows that the maximum relative error is on the same order, which is 0.32%. On the other hand, $\|w_d\|_{\ell^2} = 12.5796$, which shows 46% increase from the previous case. However, if we raise the number of point sources to 300, the radiating effort and relative error both remain in the same order as in the first experiment indicating that more sources ease up the total radiating effort. Further, positioning the center of the control region to $[7, -4, -4]$, so that the distance between the point sources and the region is about five wavelengths, we observe that the relative error is kept at the same order, which is 0.29%, and the radiating effort of the point sources rises to $\|w_d\|_{\ell^2} = 27.4611$. Hence, the simulation suggests that the control points may be placed further away from the sources, however, this may increase the power required to be radiated by the sources.

3.2. Point sources are placed at least 10 wavelengths from the obstacle and the control region is behind the obstacle, i.e., Let $\mathbf{y}_j$, $j = 1, \dots, N$ be the point sources and if we have $|\mathbf{y}_j| \gg |\mathbf{z}|$ for every $j = 1, \dots, N$, $\mathbf{z} \in W$, we can use the far-field approximation to see that

$$\frac{e^{ik|\mathbf{z}-\mathbf{y}_j|}}{4\pi|\mathbf{z}-\mathbf{y}_j|} \approx \frac{e^{ik|\mathbf{y}_j|}}{|\mathbf{y}_j|} \cdot e^{-ik\mathbf{z}\cdot\hat{\mathbf{y}}_j} \tag{3.9}$$

and with the plane wave representation, Laplace spherical functions, and addition theorem, we get

$$e^{-ik\mathbf{z}\cdot\hat{\mathbf{y}}_j} = 4\pi \sum_{n=0}^{\infty} \sum_{m=-n}^{n} i^n j_n(k|\mathbf{z}|) Y_n^m(\hat{\mathbf{z}}) \overline{Y_n^m(-\hat{\mathbf{y}}_j)}. \tag{3.10}$$

Hence, we see that with these configurations, the incident field may be expressed as

$$u_{inc}(\mathbf{z}) = \sum_{j=1}^{N} 4\pi \frac{e^{ik|\mathbf{z}-\mathbf{y}_j|}}{4\pi|\mathbf{z}-\mathbf{y}_j|} \approx \sum_{j=1}^{N} \frac{e^{ik|\mathbf{y}_j|}}{|\mathbf{y}_j|} \cdot \sum_{n=0}^{\infty} \sum_{m=-n}^{n} i^n j_n(k|\mathbf{z}|) Y_n^m(\hat{\mathbf{z}}) \overline{Y_n^m(-\hat{\mathbf{y}}_j)}, \tag{3.11}$$

and the scattered field u_s is obtained as before given by (3.6) and (3.7). In this section, we place the center of the 150 point sources to $[4, 0, -5]$ with radius of support 0.7 so that the sources are at least 10 wavelengths away from the obstacle and define the control region by

$$W = \left\{ (r, \theta, \phi) \in \mathbb{R}^3 : r \in [1, 1.5], \theta \in \left[\frac{7\pi}{8}, \frac{11\pi}{10} \right], \phi \in \left[\frac{17\pi}{64}, \frac{63\pi}{128} \right] \right\}, \tag{3.12}$$

and move its center to $[-0.75, 0, 0.75]$ so that the region is about one wavelength behind the obstacle, and represent this again using 580 collocation points. This geometry is conveyed in Figure 6 (where a 2D sketch of the 3D geometry is rendered).

In Figure 7, we can see the generated and prescribed field on a shifted mesh of W with the maximum relative error of 0.33% on W while $\|w_d\|_{\ell^2} = 1172.4$. Figure 8 shows the radiating effort contribution of each point source. Meanwhile, in Figure 9, we show the interpolated values for the prescribed and generated acoustic field on the cross section $x = -1.90$ of the control region W. If we take the control region closer to the obstacle, we see that we may be able to keep the pointwise

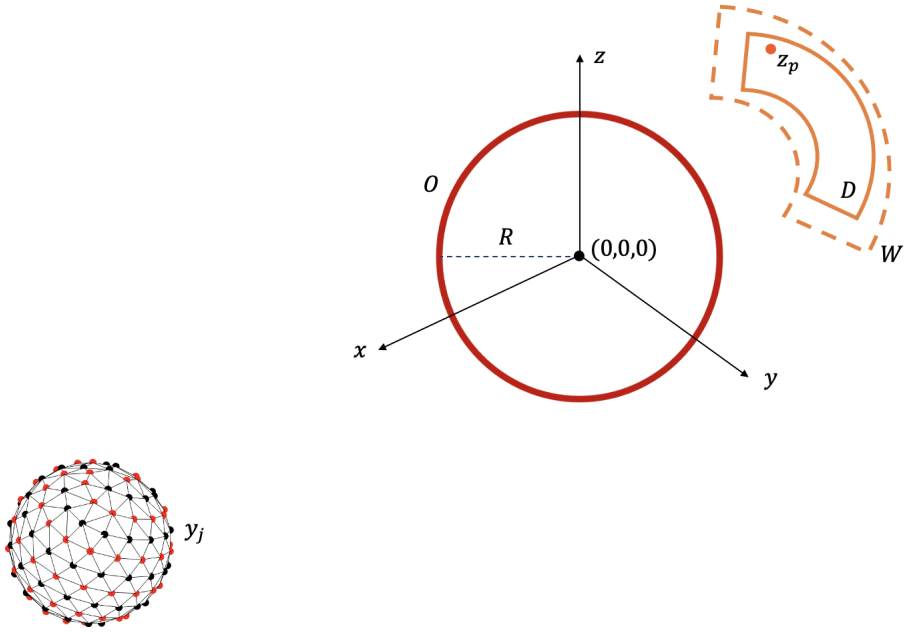

FIGURE 6. Geometry of the numerical scheme

relative error on the same order, however, one needs to increase the radiated effort of the point sources.

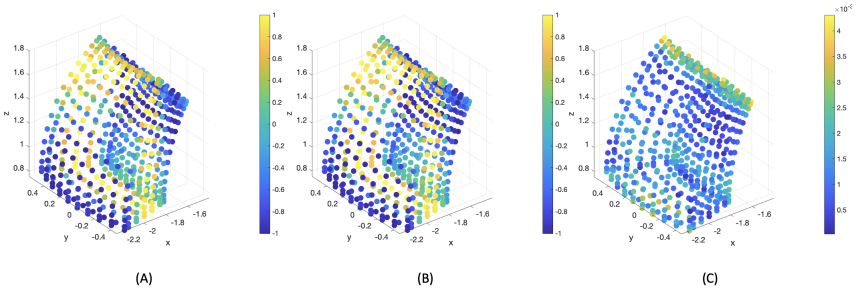

FIGURE 7. Real parts of the (A) generated and (B) prescribed fields on a shifted mesh of W, and (C) the pointwise relative error on W if the control region is one wavelength away behind the obstacle

In fact, if we move the region to about half a wavelength behind the obstacle, we observe that we can keep the error to a maximum of order 10^{-2} but $\|w_d\|_{\ell^2} = 1.1153 \times 10^6$, which is about 950% increase compared to the previous case and placing it as close as a quarter of a wavelength from the obstacle, we observe that the maximum relative error is 4.47% while the radiating effort increased by more than 200% to $\|w_d\|_{\ell^2} = 3.7357 \times 10^6$.

In Table 1, we note that we can keep the maximum pointwise relative error of the simulation and lower the total power required to be radiated if we increase the

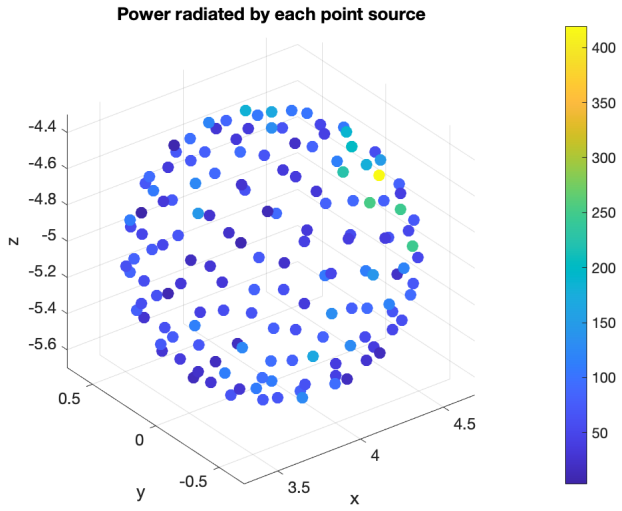

FIGURE 8. Power radiated by each point source $\mathbf{y}_j$ (magnitude)

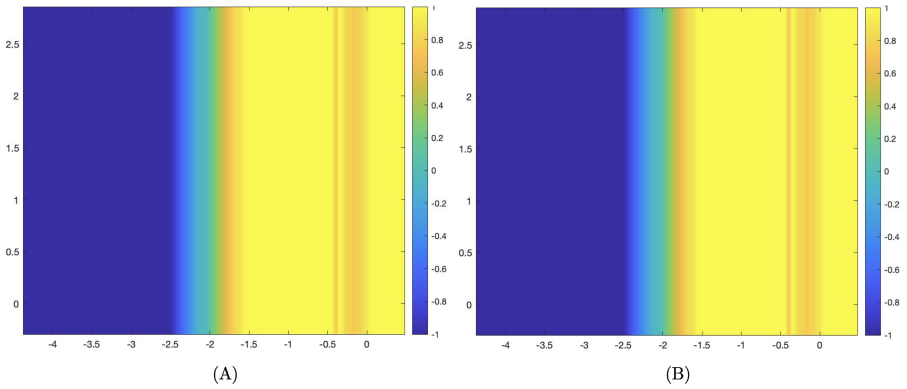

FIGURE 9. (A) Desired and (B) generated fields on a cross section of W

number of point sources. In fact, if we enlarge the control region in the azimuthal direction to $\theta \in \left[\frac{3\pi}{4}, \frac{4\pi}{5}\right]$, we see that there is a significant increase in radiating effort but maybe reduced if we increase the number of point sources radiating the acoustic field. If we further expand the size of the control region, with $\theta \in \left[\frac{3\pi}{4}, \frac{4\pi}{5}\right]$ and $\phi \left[\frac{5\pi}{32}, \frac{39\pi}{64}\right]$, we may observe that the power demand grow to order of 10^6 and the maximum relative error also rose to an order of 10^{-2} from 10^{-3} when computed for a smaller control region.

Thus, we take note that a constructing a larger control region requires greater power or more point sources to sustain the maximum pointwise relative error in the same order.

TABLE 1. Increase in the size of control region, associated power, point sources, and maximum pointwise relative error

θ	ϕ	No. of point sources	$\|w_d\|_{\ell^2}$	Max. rel. error
$\left[\frac{7\pi}{8}, \frac{11\pi}{10}\right]$	$\left[\frac{17\pi}{64}, \frac{63\pi}{128}\right]$	150	1.1724×10^3	0.33%
		250	7.5120×10^2	0.33%
		300	6.4987×10^2	0.33%
$\left[\frac{3\pi}{4}, \frac{4\pi}{5}\right]$	$\left[\frac{17\pi}{64}, \frac{63\pi}{128}\right]$	150	5.9566×10^3	0.32%
		250	3.9716×10^3	0.31%
		300	3.3282×10^3	0.31%
$\left[\frac{3\pi}{4}, \frac{4\pi}{5}\right]$	$\left[\frac{5\pi}{32}, \frac{39\pi}{64}\right]$	150	8.2482×10^6	6.87%
		250	3.5576×10^6	2.17%
		300	5.2951×10^6	3.46%

REMARK 3.1. We note that for all the simulations above, we use a sound-soft obstacle O, however, sound-hard obstacles may be treated similarly.

4. Conclusion

In this report, we presented a first theoretical argument and numerical support to characterize a given source such that its radiated field approximates desired patterns in prescribed exterior regions and given far field directions in environments with known impenetrable obstacles.

Our current numerical simulations suggest that in an environment with known obstacles it is possible to build an active scheme for the localization of acoustic energy while preserving desired far field behavior in given directions with applications to covert communications in the presence of obstacles, energy localization behind an obstacles with applications to imaging and interference or localized communication with dynamic quiet regions.

Our next work will be focused on considering a detailed theoretical and general sensitivity analysis for the case where general sound soft, sound hard, and penetrable obstacles are considered together with mutual coupling between obstacles as well as coupling with the antenna.

References

[1] Jens Ahrens. *Analytic Methods of Sound Field Synthesis*. T-Labs Series in Telecommunications Services. Springer, 2012.

[2] Jens Ahrens. *Analytic Methods of Sound Field Synthesis*. Springer, 2012.

[3] Jens Ahrens and Sascha Spors. Sound field reproduction using planar and linear arrays of loudspeakers. *IEEE Transactions on Audio, Speech, and Language Processing*, 18(8):2038–2050, 2010.

[4] Takuma Okamoto andAtsushi Sakaguchi. Experimental validation of spatial fourier transform-based multiple sound zone generation with a linear loudspeaker array. *The Journal of the Acoustical Society of America*, 141:1769–1780, 2017.

[5] Thomas S. Angell and Andreas Kirsch. *Optimization Methods in Electromagnetic Radiation*. Springer Monographs in Mathematics. Springer-Verlag New York, 2004.

[6] Yuri Bobrovnitskii. Impedance acoustic cloaking. *New J. Phys*, 12:043049, 2010.

[7] Charles Allan Boyles. *Acoustic waveguides: applications to oceanic science*. Wiley- Interscience, 1984.

[8] O. M. Bucci, A. Capozzoli, and G. D'Elia. Power pattern synthesis of reconfigurable conformal arrays with near-field constraints. *IEEE Trans. on Antennas and Prop.*, 52(1), 2004.

[9] James L. Buchanan, Robert P. Gilbert, Armand Wirgin, and Yongzhi S. Xu. *Marine Acoustics: Direct and Inverse Problems*. SIAM, 2004.
[10] Jordan Cheer. Active control of scattered acoustic fields: cancellation, reproduction and cloaking. *J. Acoust. Soc. Am.*, 140(3):1502–1512, 2016.
[11] Jordan Cheer and Stephen J. Elliott. Multichannel control systems for the attenuation of interior road noise in vehicles. *Mech. Syst. Signal Process.*, 60-61:753–769, 2015.
[12] S. Clauzier, S. M. Mikki, and Y. M. M. Antar. Design of near-field synthesis arrays through global optimization. *IEEE Transactions on Antennas and Propagation*, 63(1):151–165, Jan 2015.
[13] David Colton and Rainer Kress. *Integral equation methods in scattering theory*. SIAM Series: Classics in Applied Mathematics, 72, 2013.
[14] Massimiliano Comisso, Giulia Buttazzoni, and Roberto Vescovo. Reconfigurable antenna arrays with multiple requirements: A versatile 3d approach. *International Journal of Antennas and Propagation*, 2017, 2017.
[15] Massimiliano Comisso and Roberto Vescovo. 3d power synthesis with reduction of near-field and dynamic range ratio for conformal antenna arrays. *IEEE Trans. on Antennas and Prop.*, 59(4), 2011.
[16] Anthony J. Devaney. *Mathematical Foundations of Imaging, Tomography and Wavefield Inversion*. Cambridge University Press, 2012.
[17] Neil Jerome A. Egarguin, Daniel Onofrei, and Eric Platt. Sensitivity analysis for the active manipulation of helmholtz fields in 3d. *Inverse Problems in Science and Engineering*, 28(3):314–339, 2020.
[18] Neil Jerome A. Egarguin, Shubin Zeng, Daniel Onofrei, and Jiefu Chen. Active control of helmholtz fields in 3d using an array of sources. *Wave Motion*, 94(102523):1–27, 2020.
[19] Neil Jerome Andal Egarguin, Daniel Onofrei, Chaoxian Qi, and Jiefu Chen. Active manipulation of helmholtz scalar fields: Near field synthesis with directional far field control. *Inverse Problems*, 2020.
[20] Daniel Egglera, Hyuck Chung, Fabien Montiel, Jie Pan, and Nicole Kessissoglou. Active noise cloaking of 2d cylindrical shells. *Wave Motion*, 87:106–112, 2019.
[21] Stephen J. Elliot, Jordan Cheer, Jung-Woo Choi, and Youngtae Kim. Robustness and regularization of personal audio systems. *IEEE Trans. of Audio, Speech, and Language process.*, 20(7):2123–2133, 2012.
[22] Stephen Elliott. *Signal Processing for Active Control*. Signal Processing and its Applications. Academic Press, 1st ed edition, 2001.
[23] Chris R. Fuller and Andreas H. von Flotow. Active control of sound and vibration. *IEEE Control Systems Magazine*, 15(6):9–19, Dec 1995.
[24] J. García-Bonito and S.J. Elliott. Active cancellation of acoustic pressure and particle velocity in the near field of a source. *Journal of Sound and Vibration*, 221(1):85 – 116, 1999.
[25] Dieter Guicking. Active control of sound and vibration history - fundamentals - state of the art. *Festschrift DPI, Universitatsverlag Gottingen*, pages 1–32, 01 2007.
[26] Zerui Han, Ming Wu, Qiaoxi Zhu, and Jun Yang. Two-dimensional multizone sound field reproduction using a wave-domain method. *The Journal of the Acoustical Society of America*, 144:1–6, 2018.
[27] Zerui Han, Ming Wu, Qiaoxi Zhu, and Jun Yang. Three-dimensional wave-domain acoustic contrast control using a circular loudspeaker array. *The Journal of the Acoustical Society of America*, 145:1–6, 2019.
[28] Mark Hubenthal and Daniel Onofrei. Sensitivity analysis for active control of the helmholtz equation. *Applied Numerical Mathematics*, 106:1–23, 2016.
[29] F.B. Jensen, W.A. Kuperman, M.B. Porter, and H. Schmidt. *Computational Ocean Acoustics*. Springer, 2011.
[30] Wenyu Jin, W. Bastiaan Kleijn, and David Virette. Multizone soundfield reproduction using orthogonal basis expansion. *2013 IEEE International Conference on Acoustics, Speech and Signal Processing*, pages 311–315, 2013.
[31] Joseph B. Keller and John S. Papadakis. *Wave Propagation and Underwater Acoustics*. Number 70 in Lecture Notes in Physics. Springer-Verlag, 1977.
[32] Sang-Myeong Kim, Joao A. Pereira, Antonio E. Turra, and Jun-Ho Cho. Modeling and dynamic analysis of an electrical helmholtz resonator for active control of resonant noise. *Journal of Vibration and Acoustics*, 139(5):1–9, 2017.

[33] L. Landesa, F. Obelleiro, J.L. Rodriguez, J.A. Rodriguez, F. Ares, and A.G. Pino. Pattern synthesis of array antennas with additional isolation of near field arbitrary objects. *Electronics Letters*, 34(16):1540–1541, 1998.
[34] P. Leug. Process of silencing sound oscillations. *U.S. patent no. 2043416*, 1936.
[35] Jingwei Liu, Xiaolin Wang, Ming Wu, and Jun Yang. An active control strategy for the scattered sound field control of a rigid sphere. *JASA*, 144(EL52), 2018.
[36] J. Lončarić, V. S. Ryaben'kii, and S. V. Tsynkov. Active shielding and control of noise. *SIAM J. Appl. Math.*, 62(2):563–596, 2001.
[37] J. Lončarić and S. V. Tsynkov. Optimization of acoustic source strength in the problem of active noise control. *SIAM J. Appl. Math*, 63(4):1141–1183, 2003.
[38] J. Lončarić and S. V. Tsynkov. Optimization of power in the problems of active control of sound. *Math. and Computers in Simulation*, 65:323–335, 2004.
[39] J. Lončarić and S. V. Tsynkov. Quadratic optimization in the problems of active control of sound. *Applied Numerical Mathematics*, 52:381–400, 2005.
[40] M. V. Lozano and F. Ares Pena. Antenna array pattern synthesis in the presence of near zone scatterers: three-dimenssional vector case. *Jour. of Electromagnetic Waves and Appl.*., 13:1493–1507, 1999.
[41] Rajabi Majid and Mojahed Alireza. Active acoustic cloaking spherical shells. *Acta Acustica united with Acustica,*, 104(1):5–12, 2019.
[42] Qibo Mao, Shengquan Li, and Weiwei Liu. Development of a sweeping helmholtz resonator for noise control. *Applied Acoustics*, 141:348 – 354, 2018.
[43] P.A. Martin. Acoustic scattering and radiation problems and the null field method. *Wave Motion*, 4(4):391–408, 1982.
[44] P.A. Martin. *Multiple Scattering Interaction of Time-Harmonic Waves with N Obstacles*. Cambridge University Press, 1st ed edition, 2006.
[45] P.A. Martin. On connections between boundary integralequations and t-matrix method. *Engineering Analysis with Boundary Elements*, 27:771–777, 2013.
[46] Dylan Menzies. Sound field synthesis with distributed modal constraints. *Acta Acust. Acust*, 98(1):15–27, 2012.
[47] D. A. B Miller. On perfect cloaking. *Opt. Express*, 14:12457–12466, 2006.
[48] P. A. Nelson and S. J. Elliott. *Active Control of Sound*. Academic London, 1992.
[49] H.F. Olson and E.G. May. Electronic sound absorber. *J. Acad. Soc. Am.*, 25:1130–1136, 1953.
[50] Akira Omoto, Shiro Ise, Yusuke Ikeda, Kanako Ueno, Seigo Enomoto, and Maori Kobayashi. Sound field reproduction and sharing system based on the boundary surface control principle. *Acoustical Science and Technology*, 36:1–11, 01 2015.
[51] Daniel Onofrei. On the active manipulation of fields and applications. i - the quasistatic regime. *Inverse problems*, 28(10):105009, 2012.
[52] Daniel Onofrei. Active manipulation of fields modeled by the helmholtz equation. *Journal Of Integral Equations and Applications*, 26(4):553–579, 2014.
[53] Daniel Onofrei and Eric Platt. On the synthesis of acoustic sources with controllable near fields. *Wave Motion*, 77:12–27, 2017.
[54] Daniel Onofrei, Eric Platt, and Neil Jerome A. Egarguin. Active manipulation of exterior electromagnetic fields by using surface sources. *Quarterly of Appl. Math*, 78(4):641–670, 2020.
[55] N. Peake and D. G. Crighton. Active control of sound. *Annu. Rev. Fluid Mech*, 32:137–164, 2000.
[56] A.W. Peterson and S.V. Tsynkov. Active control of sound for composite regions. *SIAM J. Appl. Math*, 67(6):1582–1609, 2007.
[57] Roy Pike and Pierre Sabatier. *Scattering and inverse scattering in pure and applied science*. Academic Press, 1st ed edition, 2002.
[58] M. A. Poletti and F. M. Fazi. An approach to generating two zones of silence with application to personal sound systems. *The Journal of the Acoust. Soc. of America*, 137:598–605, 2015.
[59] B.I. Popa, D. Shinde, A. Konneker, and S. A. Cummer. Active acoustic metamaterials reconfigurable in real time. *Phys. Rev. B*, 91, 2015.
[60] Gary Roach and Rainer Kress. On mixed boundary value problems for the Helmholtz equation. *Proceedings of the Royal Society of Edinburgh*, 77:65–77, 1976.
[61] J. A. Rodriguez, M. V. Lozano, and F. Ares Pena. Antenna array pattern synthesis in the presence of near zone scatterers: two-dimenssional scalar case. *Microwave and Opt. Tech. Lett.*., 21(4), 1999.

[62] Gálvez Marcos F. Simón, Menzies Dylan, and Fazi Filippo Maria. Dynamic audio reproduction with linear loudspeaker arrays. *JAES*, 67(4):190–200, 2019.
[63] P.A. Nelson S.J. Elliot. The active control of sound. *Electronics and Comm. Engineering Journal*, 1990.
[64] Leun Tsang, Jin Au Kong, and Kung-Hau Ding. *Scattering of electromagnetic waves*. Wiley, 1st ed edition, 2000.
[65] Fernando Guevara Vasquez, Graeme W. Milton, and Daniel Onofrei. Active exterior cloaking. *Phys. Rev. Lett.*, 103:073901, 2009.
[66] Fernando Guevara Vasquez, Graeme W. Milton, and Daniel Onofrei. Broadband exterior cloaking. *Optics Express*, 17(17):14800–14805, 2009.
[67] Fernando Guevara Vasquez, Graeme W. Milton, and Daniel Onofrei. Exterior cloaking with active sources in two dimensional acoustics. *Wave Motion*, 48:515–524, 2011.
[68] Junqing Zhang, Wen Zhang, Thushara D. Abhayapala, Jingli Xie, and Lijun Zhang. 2.5d multizone reproduction with active control of scattered sound fields. *IEEE Explore*, ICASSP 2019 - 2019 IEEE International Conference on Acoustics, Speech and Signal Processing (ICASSP):141–145, 12-17 May 2019.
[69] Wen Zhang, Thushara D. Abhayapala, Terence Betlehem, and Filippo Maria Fazi. Analysis and control of multi-zone sound field reproduction using modal-domain approach. *J. Acoust. Soc. Am.*, 140(3):2134–2144, 2016.
[70] Qiaoxi Zhu, Philip Coleman, Xiaojun Qiu, Ming Wu, Jun Yang, and Ian S. Burnett. Robust personal audio geometry optimization in the svd-based modal domain. *IEEE/ACM Transactions on Audio, Speech, and Language Processing*, 2018.

Department of Mathematics, University of Houston, Texas 77004
Current address: Department of Mathematics, University of Houston, Texas 77004
E-mail address: lybesabe@uh.edu

Department of Mathematics, University of Houston, Texas 77004
E-mail address: dtonofre@central.uh.edu